Composite Scattering Study of Layered Rough Surface with Target based on CCIA

Jiaguo Zhang and Huan Wei

School of Mathematics and Computer Science
Yichun University, Yichun, 336000, China
ycu_zjg2022@126.com, wbsf2019@126.com

***Abstract* –** In this paper, a fast Cross Coupling iterative Approach (CCIA) is proposed for studying the composite scattering of the layered rough surfaces with buried target, which uses forward backward method (FBM) to solve the electric field integral equations (EFIE) of the layered rough surface and bi-conjugate gradient method (BI-CG) to solve the EFIE of the target, and the interaction between the rough surface and the target is achieved by updating the excitation term. The algorithm is applied to calculate the composite scattering coefficients of the rough surface with a buried target, the results match with those of the traditional numerical algorithm MOM while the error can be reduced to 10^{-3} by 6 iterations, and the convergence speed and calculation accuracy meet the requirements. The composite scattering coefficients and Angular Correlation Function (ACF) amplitudes of layered rough surface and dielectric targets with different conditions are calculated, and the effects of various factors such as target size and burial depth on the composite scattering characteristics are discussed. It is found that the buried targets will have a great influence on the scattering characteristics, weakening or neglecting the coupling between them will lead to larger errors. Moreover, the results show that ACF can suppress scattering from rough surfaces well, making the scattering characteristics of the target more obvious, which is important for detecting underground targets.

***Index Terms* –** Cross Coupling iterative Approach (CCIA), Electric Field Integral Equations (EFIE), Angular Correlation Function (ACF), composite scattering characteristics.

I. INTRODUCTION

The study of electromagnetic characteristics [1–5] of targets and environment has a very important role in the field of remote sensing information processing and target identification: in the field of remote sensing information processing [6–9], it is necessary to analyze and study the electromagnetic characteristics of remote sensing environment and targets, and to design and manufacture sensors to match them in order to obtain the best target remote sensing information. Radar is one of the most commonly used sensors for target remote sensing, which uses electromagnetic signals to sense targets and has the ability to work around the clock. Therefore, analyzing and acquiring target and environment features, and establishing a database of target and environment features are very important for remote sensing information processing. On the other hand, target and environment feature extraction and identification [10–13] is the basic technology to realize battlefield precision perception, precision strike and missile attack and defense confrontation, so target feature signal extraction and identification technology is the advanced stage of target and environment feature research, target and environment electromagnetic scattering feature analysis is the basis of target identification, and the model-based target identification method depends largely on the target and environment electromagnetic scattering feature modeling accuracy. There are usually two methods to obtain environmental and target characteristics: real measurements and simulations. Although the results of real measurements are highly reliable, the cost of real measurements is high and it is difficult to obtain complete scattering characteristics data due to many practical conditions. With the rapid development of computer technology, it is becoming easier and easier to realize 3D reconstruction of complex targets and high accuracy of electromagnetic calculation problems by using its powerful computing power.

Zou [14] introduced the single integral equation-Kirchhoff approximation (SIE-KA) hybrid method with a multilevel fast multipole algorithm (MLFMA) to accelerate the computation to solve complex scattering problems in coastal environments containing conductor and dielectric targets, and presented many practical ideas in remote sensing. Liang [15] established a composite scattering model based on the propagation-inside-layer expansion + generalized forward-backward method (EPILE+GFBM), studied the coupling mechanism between sea surface-missile-ship, and discussed the

Submitted On: June 5, 2023
Accepted On: November 27, 2023

https://doi.org/10.13052/2023.ACES.J.381105

effects of different states of the target (such as attitude, position, and rotation angle) on the composite scattering characteristics. The results of the study are instructive for target detection, identification, and imaging in the marine environment. Zou [16] established a natural valley model, simulated the cavity structure of the valley, and proposed the SBR-EEC method to solve the compound scattering problem existing in ultra-low altitude targets in the valley. It is found that the cavity in the valley has a great influence on the composite scattering, which will affect the detection and identification accuracy of targets in the environment. Based on the traditional FBAM and GO/PO hybrid methods, Li [17] proposed an acceleration algorithm that can effectively reduce the occlusion judgment. Experiments prove that the algorithm is effective for SAR imaging of ships in the marine environment, and the electromagnetic scattering characteristics of multi-ship targets in the marine environment are studied based on the algorithm. Wang [18] proposed an algorithmic model for composite scattering of environment with target, derived the integral equations for each computational domain in the complex model, solved them one by one using a hybrid method of CFIE and EFIE, and accelerated the matrix computation using the multilevel fast multipole algorithm (MLFMA) in the computation process.

In this paper, we focus on the composite scattering problem of layered rough surface with target. Firstly, in order to solve the problem of low computational efficiency of traditional algorithms, the CCIA algorithm is proposed, which uses FBM to solve the EFIE of the layered rough surface and BI-CG to solve the EFIE of the target, and the interaction between the rough surface and the target is achieved by updating the excitation term. And the effectiveness of the proposed algorithm is demonstrated by computational examples. Then the coupling effect between the rough surface and the target is studied by this algorithm, and their composite scattering coefficients are calculated, it is found that the coupling effect has a great influence on the composite scattering. Finally, the ACF of the composite environment is investigated, and the results show that the ACF is greatly influenced by the target size, and the ACF can well suppress the scattering from rough surfaces, which is important for detecting subsurface targets.

II. COMPOSITE SCATTERING CALCULATION MODEL

A. Coupled boundary integral equations of layered rough surface and dielectric target

A typical spherical medium target is located in zone II, the second layer of the medium, as shown in Fig. 1. Zone O denotes free space, usually air; Zone I denotes rough surface 1 and Zone II denotes rough surface 2, which usually have different dielectric constants.

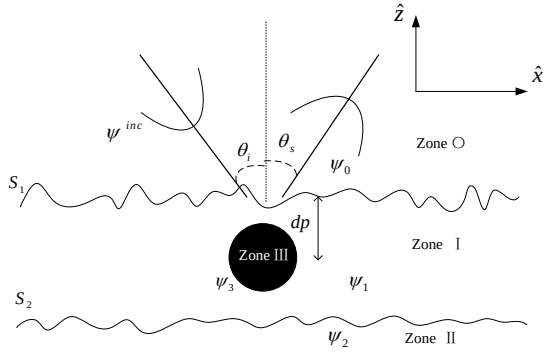

Fig. 1. Graphics of dielectric target and rough surfaces.

When the size of the target is infinitely small (which can be considered as no target), the boundary integral equation of the stratified rough surface is:

$$\frac{1}{2}\psi_0(r) = \psi^{inc}(r) + \int_{f_1(x)} \left[\psi_0(r)\hat{n}_1 \cdot \nabla g_0\left(r,r'\right) - g_0\left(r,r'\right)\hat{n}_1 \cdot \nabla\psi_0(r)\right] ds, \quad (1)$$

$$\frac{1}{2}\psi_1(r) = \int_{f_2(x)} \left[\psi_1(r)\hat{n}_2 \cdot \nabla g_1\left(r,r'\right) - g_1\left(r,r'\right)\hat{n}_2 \cdot \nabla\psi_1(r)\right] ds - \int_{f_1(x)} \left[\psi_1(r)\hat{n}_1 \cdot \nabla g_1\left(r,r'\right) - g_1\left(r,r'\right)\hat{n}_1 \cdot \nabla\psi_1(r)\right] ds, \quad (2)$$

$$\frac{1}{2}\psi_1(r) = \int_{f_2(x)} \left[\psi_1(r)\hat{n}_2 \cdot \nabla g_1\left(r,r'\right) - g_1\left(r,r'\right)\hat{n}_2 \cdot \nabla\psi_1(r)\right] ds. \quad (3)$$

In the above equation, $\hat{n}_i$ is the normal vector in zone i with the direction vertically upward, $\boldsymbol{r}$ represents the field point, $\boldsymbol{r'}$ represents the source point, $g_i(r,r')$is the Green's function in zone i, and there is

$$r = x\hat{x} + z\hat{z}, \quad (4)$$

$$r' = x'\hat{x} + z'\hat{z}, \quad (5)$$

$$g_i(r,r') = \frac{i}{4}H_0^{(1)}(k_i\left|r-r'\right|). \quad (6)$$

The target surface is denoted by f_c and the rough surface is denoted by $f_i(x)(i = 2,3$ denotes the upper and lower rough surfaces, respectively). ψ^{inc} denotes the incident wave and ψ_i is the total field in the i region.

And when there is a non-negligible target (sphere) on the stratified rough surface, Eq. (2) can be rewritten as

$$\frac{1}{2}\psi_1(r) = \int_{f_2(x)} \left[\psi_1(r)\hat{n}_2 \cdot \nabla g_1\left(r,r'\right) - g_1\left(r,r'\right)\hat{n}_2 \cdot \nabla\psi_1(r)\right] ds - \int_{f_1(x)} \left[\psi_1(r)\hat{n}_1 \cdot \nabla g_1\left(r,r'\right) - g_1\left(r,r'\right)\hat{n}_1 \cdot \nabla\psi_1(r)\right] ds + \int_{f_0} \left[\psi_1(r)\hat{n}_{op} \cdot \nabla g_1\left(r,r'\right) - g_1\left(r,r'\right)\hat{n}_{op} \cdot \nabla\psi_1(r)\right] ds. \quad (7)$$

where $\hat{n}_{op}$ is the normal vector of the target surface with the direction perpendicular to the target surface outward,

and this partial integral in Eq. (7) represents the target's contribution to the total field.

The scattered field within the target is:

$$\frac{1}{2}\psi_3(r) = -\int_{f_0}[\psi_3(r)\hat{n}_{op}\cdot\nabla g_3(r,r') - g_3(r,r')\hat{n}_{op}\cdot\nabla\psi_3(r)]ds. \tag{8}$$

Then we obtained the surface integral equations for the stratified rough surface and the medium target. Their boundary conditions under TM and TE waves are as follows, respectively. TE:

$$\psi_i(r) = \psi_{i+1}(r)\ \frac{\partial\psi_i(r)}{\partial n_i} = \frac{\mu_i}{\mu_{i+1}}\frac{\partial\psi_{i+1}(r)}{\partial n_{i+1}}, \tag{9}$$

TM:

$$\psi_i(r) = \psi_{i+1}(r)\ \frac{\partial\psi_i(r)}{\partial n_i} = \frac{\varepsilon_i}{\varepsilon_0}\frac{\partial\psi_{i+1}(r)}{\partial n_{i+1}}. \tag{10}$$

Using the basis function to discrete the above set of equations, let the length of the rough surface is L, the discrete density is Δx, and the total discrete number is N; the dielectric target surface discrete density is Δx_0, and the total discrete number is M. The following matrix equation can be obtained:

$$A^{(0,1,1)}U_1 + B^{(0,1,1)}\psi_1 = \psi^{inc}, \tag{11}$$

$$\rho_1 A^{(1,2,1)}U_1 + B^{(1,2,1)}\psi_1 + A^{(1,2,2)}U_1 + B^{(1,2,2)}\psi_1, + C\cdot U_0 + D\cdot\psi_0 = 0, \tag{12}$$

$$\rho_1 A^{(1,2,1)}U_1 + B^{(1,2,1)}\psi_1 + A^{(1,2,2)}U_1 + B^{(1,2,2)}\psi_1, + E\cdot U_0 + F\cdot\psi_0 = 0, \tag{13}$$

$$\rho_2 A^{(2,2,2)}U_1 + B^{(2,2,2)}\psi_1 = 0, \tag{14}$$

$$G\cdot U_1 + H\cdot\psi_1 + I\cdot U_2 + J\cdot\psi_2 + K\cdot U_0 + L\cdot\psi_0 = 0, \tag{15}$$

$$\rho_3 P\cdot U_0 + Q\cdot U_0 = 0. \tag{16}$$

Where the expressions of the matrix elements $A_{mn}^{(a,b,c)}$, $B_{mn}^{(a,b,c)}$ are

$$A_m^{(a,b,c)} = \begin{cases} w^{(a,c)}\frac{i\Delta x}{4}H_0^{(1)}\left(k_a \mid r_{m,b} - r_{n,c}\right)\Delta l_{m,b} \\ (\text{for}(b=c, m\neq n) \text{ or } b\neq c) \\ w^{(a,c)}\frac{i\Delta x}{4}\left[1 + \frac{i2}{\pi}\ln\left(\frac{e^{\gamma}k_a\Delta x\Delta l_{m,b}}{4e}\right)\right] \\ (\text{for}(b=c, m=n)) \end{cases}, \tag{17}$$

$$B_{mn}^{(a,b,c)} = \begin{cases} -w^{(a,c)}\frac{ik_a\Delta x}{4}\frac{H_1^{(1)}\left(k_a\left|r_{m,b}-r_{n,c}\right|\right)}{\left\|r_{m,b}-r_{n,c}\right\|}\times \\ \left(f_c'(x_n)(x_n - x_m) - (f_c(x_n) - f_b(x_m))\right) \\ (\text{for}(b=c, m\neq n) \text{ or } b\neq c) \\ \frac{1}{2} - w^{(a,c)}\frac{f_b''(x_m)}{4\pi}\frac{\Delta x}{1+f_b'(x_m)^2} \\ (\text{for}(b=c, m=n)) \end{cases}. \tag{18}$$

Where when $a = c$, $w^{(a,c)} = 1$; when $a \neq c$, $w^{(a,c)} = -1$. And $\rho_l = \mu_l/\mu_{l-1}$ for TE wave, $\rho_l = \varepsilon_l/\varepsilon_{l-1}$ for TE wave, $U_i(x) = \frac{\partial\psi_i(r)}{\partial n'}\sqrt{1+(\partial S_l/\partial x)^2}\Big|_{r\in S_i}$, $\psi_i(x) = \psi_i(r)|_{r\in S_i}$. The three superscripts in the upper right corner of the matrix elements represent: the first number indicates the region, the second number indicates the rough surface where the field point is located, and the third number indicates the rough surface where the source point is located. The specific meaning of each parameter can be found in the literature (19), which is not repeated here considering the length of the article.

Solving the above matrix equations yields composite electromagnetic scattering results for rough surfaces and targets, and it should be noted that computational accuracy and computational time should be considered when solving. However, since the MoM numerical method [20-22] is based on strict Maxwell equations and boundary conditions, it includes various interactions between electromagnetic waves and rough surfaces (especially multiple scattering between cells on rough surfaces), and is theoretically an accurate solution method that has been widely used in scattering calculations. However, numerical simulations of scattering from rough surfaces often need to consider taking a sufficiently long rough surface for the calculation, especially under the conditions of low grazing angle incidence and moderate rough surface, where a large unknown quantity is generated after the dissection, making the conventional MoM a great challenge. For this reason, relevant fast algorithms must be used to accelerate the calculation.

B. Cross coupling iterative approach (CCIA)

Therefore, in order to solve this problem and improve the practicality of the algorithm, Cross Coupling iterative Approach (CCIA) is proposed in this paper, which overcomes the limitations of the traditional MoM by considering both the computational accuracy and the computational speed in solving the composite scattering of the layered rough surface and the medium target. The basic principle is that while considering the interaction between the layered rough surface and the dielectric target, the surface integral equation of the layered rough surface is solved by FBM and the surface integral equation of the target is solved by Bi-CG, and then the set of equations is solved by iteration. the computational volume and memory required by the CCIA method is only $O(N^2)$, which greatly improves the computational efficiency.

Rectifying Eqs. (11-16), the following matrix equation can be obtained:

$$\begin{bmatrix} A^{(0,1,1)} & B^{(0,1,1)} & 0 & 0 \\ \rho_1 A^{(1,1,1)} & B^{(1,1,1)} & A^{(1,1,2)} & B^{(1,1,2)} \\ \rho_1 A^{(1,2,1)} & B^{(1,2,1)} & A^{(1,2,2)} & B^{(1,2,2)} \\ 0 & 0 & \rho_2 A^{(2,2,2)} & B^{(2,2,2)} \end{bmatrix}\cdot\begin{bmatrix} U_1 \\ \psi_1 \\ U_2 \\ \psi_2 \end{bmatrix} = \begin{bmatrix} \psi^{inc} \\ \psi_{Tar}^1 \\ \psi_{Tar}^2 \\ 0 \end{bmatrix}, \tag{19}$$

$$\begin{bmatrix} K & L \\ \rho_3 P & Q \end{bmatrix}\begin{bmatrix} U_0 \\ \psi_0 \end{bmatrix} = \begin{bmatrix} \psi^{sur} \\ 0 \end{bmatrix}. \tag{20}$$

Where

$$\psi_{Tar}^1 = -C^I\cdot U_0 - D^I\cdot\psi_0, \tag{21}$$

$$\psi_{Tar}^2 = -E\cdot U_0 - F\cdot\psi_0, \tag{22}$$

$$\psi^{Sur} = -F^{(1)} \cdot U_1 - H^{(1)} \cdot \psi_1 - I^{(2)} \cdot U_2 - J^{(2)} \cdot \psi_2. \quad (23)$$

In the above equations, the surface current distributions of the stratified rough surface and the target can be obtained by solving the matrix Eqs. (19) and (20), respectively. ψ^i_{Tar} denotes the scattering effect of the target on the rough surface, superscript i=1 denotes the upper rough surface, superscript i=2 denotes the lower rough surface; ψ^{Sur} denotes the scattering effect of the layered rough surface on the target. Thus, the rough surface and the target do not exist in isolation, they are not only irradiated by the incident waves, but also influence each other.

During the iteration, the excitation term on the right-hand side of the matrix Eqs. (19-20) are continuously updated and Eqs. (19-20) become:

$$Z^0 \cdot I_0^{(i)} = \begin{bmatrix} A^{(0,1,1)} & B^{(0,1,1)} & 0 & 0 \\ \rho_1 A^{(1,1,1)} & B^{(1,1,1)} & A^{(1,1,2)} & B^{(1,1,2)} \\ \rho_1 A^{(1,2,1)} & B^{(1,2,1)} & A^{(1,2,2)} & B^{(1,2,2)} \\ 0 & 0 & \rho_2 A^{(2,2,2)} & B^{(2,2,2)} \end{bmatrix} \cdot \begin{bmatrix} U_1^{(i)} \\ \psi_1^{(i)} \\ U_2^{(i)} \\ \psi_2^{(i)} \end{bmatrix} = \begin{bmatrix} \psi^{inc} \\ \psi^1_{Tar}(i) \\ \psi^2_{Tar}(i) \\ 0 \end{bmatrix} = V_0^{(i)}, \quad (24)$$

$$Z^1 \cdot I_1^{(i)} = \begin{bmatrix} K & L \\ \rho_3 P & Q \end{bmatrix} \begin{bmatrix} U_0^{(i)} \\ \psi_0^{(i)} \end{bmatrix} = \begin{bmatrix} \psi^{sur}(i) \\ 0 \end{bmatrix}. \quad (25)$$

Where the upper corner marker i denotes the number of iteration steps, $I_0^{(i)}$ denotes the current distribution on the rough surface, $I_1^{(i)}$ denotes the current distribution on the target surface, $\psi^1_{Tar}(i)$ denotes the target excitation on the upper rough surface, $\psi^2_{Tar}(i)$ denotes the target excitation on the lower rough surface, and $\psi^{sur}(i)$ denotes the target excitation on the layered rough surface.

Then, each matrix is decomposed into three parts, namely the upper matrix $\boldsymbol{U}$, the lower matrix $\boldsymbol{D}$ and the diagonal matrix $\boldsymbol{L}$, and the forward backward method (FBM) method is used to solve Eq.(24), and the equations for the forward current are:

$$A^{L,(0,1,1)}U_1^f + B^{L,(0,1,1)}\psi_1^f = \psi^{inc} - \psi^{Tar} - A^{D,(0,1,1)}(U_1^f + U_1^b) - B^{D,(0,1,1)}(\psi_1^f + \psi_1^b), \quad (26)$$

$$\rho_1 A^{L,(1,1,1)}U_1^f + B^{L,(1,1,1)}\psi_1^f + A^{L,(1,1,2)}U_2^f + B^{L,(1,1,2)}\psi_2^f = \psi^1_{Tar} - \rho_1 A^{D,(1,1,1)}(U_1^f + U_1^b) - B^{D,(1,1,1)}(\psi_1^f + \psi_1^b) - A^{D,(1,1,2)}(U_2^f + U_2^b) - B^{D,(1,1,2)}(\psi_2^f + \psi_2^b), \quad (27)$$

$$\rho_1 A^{L,(1,2,1)}U_1^f + B^{L,(1,2,1)}\psi_1^f + A^{L,(1,2,2)}U_2^f + B^{L,(1,2,2)}\psi_2^f = \psi^2_{Tar} - \rho_1 A^{D,(1,2,1)}(U_1^f + U_1^b) - B^{D,(1,2,1)}(\psi_1^f + \psi_1^b) - A^{D,(1,2,2)}(U_2^f + U_2^b) - B^{D,(1,2,2)}(\psi_2^f + \psi_2^b), \quad (28)$$

$$\rho_2 A^{L,(2,2,2)}U_1^f + B^{L,(2,2,2)}\psi_1^f = -\rho_2 A^{D,(2,2,2)}(U_2^f + U_2^b) - B^{D,(2,2,2)}(\psi_2^f + \psi_2^b). \quad (29)$$

Where $U_l = U_l{}^f + U_l{}^b$, $\psi_l = \psi_l{}^f + \psi_l{}^b$, f and b denote the forward and backward components obtained after decomposition of the unknown components, respectively.

The initial values of the iteration are $U_1^{b,(0)} = 0$, $\psi_1^{b,(0)} = 0$, $U_2^{b,(0)} = 0$, $\psi_2^{b,(0)} = 0$, the initial values are substituted into Eq. (24) to update the solution to obtain U_1, ψ_1, U_2 and ψ_2. Then U_1, ψ_1, U_2, ψ_2 are substituted into Eq. (25) to obtain U_0, and the updated ψ^1_{Tar} and ψ^2_{Tar} are calculated and then substituted into Eq. (24). Repeat this iterative process until the specified convergence accuracy is reached. Eq. (24) can be solved by the FBM method, while Eq. (25) needs to be solved by the bi-conjugate gradient method (Bi-CG). The iteration error of step i is:

$$\tau(i) = \left| \frac{Z^1 \cdot [I_1^{(i)} - I_1^{(i-1)}]}{V_1^{(i)}} \right|. \quad (30)$$

The calculation achieves multiple scattering calculations of the layered rough surface and the target by continuously updating the excitation terms of the two equations until the iterative error meets the specified convergence accuracy.

C. Conical incident wave

In order to apply the numerical algorithm, the area calculated by the rough surface is bounded in a certain range. For the two-dimensional scattering problem, in order to limit the rough surface to L, i.e., $|x| \le L/2$, the surface current is artificially specified to be zero when $|x| > L/2$. In this way, the surface current has a sudden change at $x = \pm L/2$, and if a plane wave is used, this will cause artificial reflections at both endpoints.

In order to solve this problem, one of the methods is to set the edge as a periodic boundary, but this method has a certain approximation, and the error is not easy to determine, so it is generally not desirable; the second method is to select the incident wave as a conical wave, that is, the incident wave has Gaussian characteristics, when close to the boundary, the incident wave tends to zero, so as to avoid the abrupt change of the surface current. Using the widely used Thorsos conical wave, which can well satisfy the Helmholtz fluctuation equation, the one-dimensional conical wave is [23]

$$\psi^{inc}(r) = \exp[ik(x\sin\theta_i - z\cos\theta_i)\cdot(1+w(r))] \cdot \exp[-\frac{(x+z\tan\theta_i)^2}{g^2}], \quad (31)$$

where θ_i is the angle of incidence (labeled in Fig. 1) and g is the beamwidth factor, which determines the width of the window function.

Figure 2 represents the distribution of the amplitude of the incident wave on the surface.

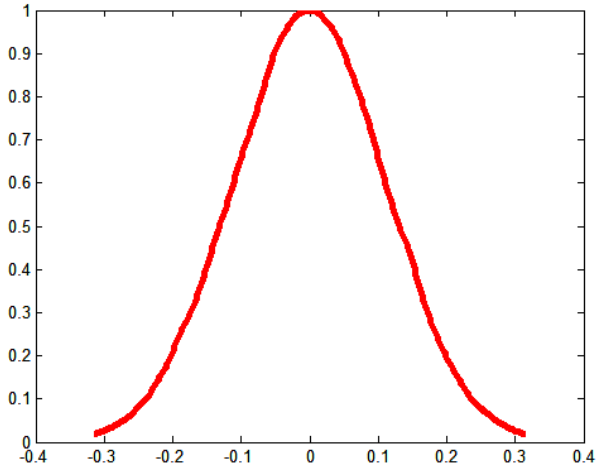

Fig. 2. Amplitude distribution of one-dimensional conical incident waves.

In Eq. (31), the wave vector of the incident wave is

$$k_i = k\left(\hat{x}\sin\theta_i - \hat{z}\cos\theta_i\right), \tag{32}$$

$$w(x,z) = \frac{1}{(kg\cos\theta_i)^2}\left[2\frac{(x+z\tan\theta_i)^2}{g^2} - 1\right]. \tag{33}$$

The width g is an important physical quantity that determines the incident width of the incident wave and the length of the rough surface. The larger the value of g, the greater the incident width of the incident wave and the greater the length of the rough surface. The larger the value of g, the more the numerical calculation can reflect the average scattering characteristics of the rough surface, and the more accurate the numerical calculation is, but it needs to consume more storage and calculation time. Therefore, the choice of g should consider both the accuracy of the calculation results and the calculation efficiency: the conical width g is determined by the incident angle, while the rough surface length L is determined by g. The expression is

$$g \geq \frac{6}{(\cos\theta_i)^{1.5}} L = 4g. \tag{34}$$

III. ALGORITHM VALIDATION

In this subsection, the parameters of the rough surface and the target are: $h_1 = 0.13\lambda$, $L_1 = 40\lambda$, $l_1 = 1.0\lambda$, $\varepsilon_{r1} = 4.0 + 0.01i$, $d = 6.0\lambda$, $h_2 = 0.08\lambda$, $L_2 = 40\lambda$, $l_2 = 1.0\lambda$, $\varepsilon_{r2} = 7.0$, $\theta_i = 20^o$, $g = L/6$, $dp = 3.0\lambda$, $R = 1.0\lambda$, $\varepsilon_c = 2.25$. Where h_i is the root mean square height of the rough surface, L_i is the length of the rough surface, l_i is the correlation length, ε_{ri} is the dielectric constant of the rough surface, where i=1 represents the upper rough surface and i=2 represents the lower rough surface, ε_c is the dielectric constant of the target, dp is the burial depth of the target, R is the radius of the sphere, and d is the thickness of the rough surface.

This subsection focuses on verifying the effectiveness of the CCIA algorithm proposed in this paper in terms of both computational efficiency and computational accuracy.

The MOM numerical algorithm is a solution method with high accuracy, and although it is relatively slow, it is undoubtedly suitable and more convincing as a validation algorithm due to its accurate calculation. In this subsection, both the algorithm of this paper and the MOM method are used to calculate the composite bistatic scattering coefficients for the layered rough surface and the dielectric target, and the calculation results are shown in Fig. 3.

Figure 3 (a) shows the calculation results of TE waves, and Fig. 3 (b) shows the calculation results of TM waves. From these two figures, it can be seen that the calculation curves of CCIA and MOM almost overlap for both TE incident wave and TM incident wave, indicat-

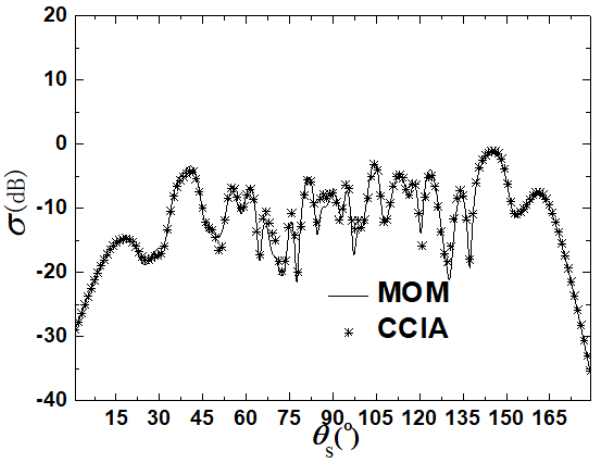

(a) TE incident wave

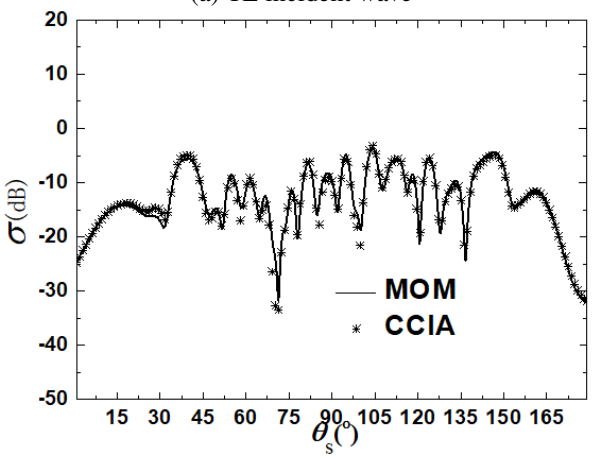

(b) TM incident wave

Fig. 3. Comparison of calculation results of different methods.

ing that their calculation results are extremely close, thus verifying the correctness of the method.

Table 1: Comparison of time consumed

Method	Time Consumption (sec)
CCIA	357
MoM	2109

Table 1 shows the time consumed for two different methods. It is evident that CCIA requires only 357 seconds of computation time, while MoM takes 2109 seconds. The CCIA method greatly reduces the computational time and significantly improves computational efficiency.

Figure 4 shows the variation of the iteration error $\tau(i)$ with the number of iteration steps i during the calculation. When CCIA is used to calculate the composite scattering of rough surfaces and targets, the iteration error in both cases can be reduced to 10^{-3} after 6 iterations, and the convergence speed is relatively fast, which can meet the calculation requirements. It indicates that the algorithm improves the computational speed while ensuring the computational accuracy, which is consistent with the expectation.

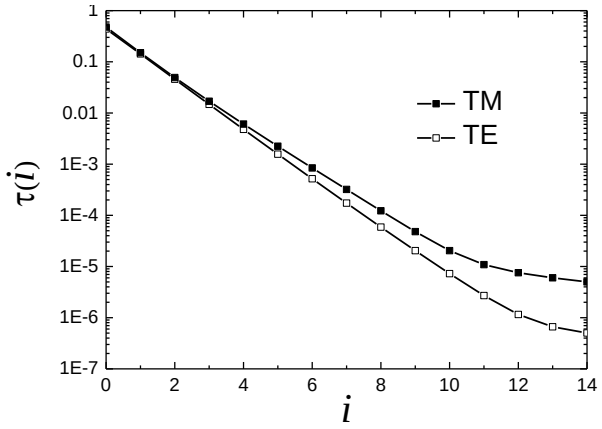

Fig. 4. Iterative error curve.

IV. CALCULATION RESULTS AND ANALYSIS

A. Effect of target on compound scattering

In this subsection, the parameters of the rough surface and the target are: $h_1 = 0.13\lambda$, $L_1 = 40\lambda$, $l_1 = 0.16\lambda$, $\varepsilon_{r1} = 4.0 + 0.01i$, $d = 6.0\lambda$, $h_2 = 0.08\lambda$, $L_2 = 40\lambda$, $l_2 = 0.16\lambda$, $\varepsilon_{r2} = 7.0$, $\theta_i = 20°$, $g = L/6$, $dp = 3.0\lambda$, $R = 1.0\lambda$, $\varepsilon_c = 2.25$.

In the study, the radii of the spheres are set as $R = 1.0\lambda$ and $R = 2.0\lambda$, respectively, and other parameters are kept constant to study the effects of different sizes of spheres on the composite scattering, and the results are shown in Fig. 5. Observing Fig. 5, it can be found that the scattering coefficient increases significantly after the introduction of the medium target relative to the rough surface without a target, which is caused by the mutual coupling effect between the target and the rough surface, and as the target volume increases, the distance between the target and the upper and lower rough surfaces shortens, the mutual coupling effect becomes stronger, and the scattering coefficient shows an enhanced trend, and the influence on the scattering characteristics of the layered rough surface becomes more and more obvious. Therefore, when studying the problems related to the target and the environment, the coupling effect between them must be taken into account.

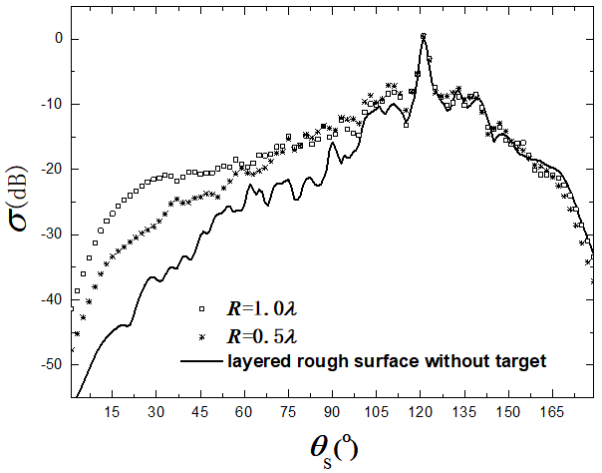

(a) TE incident wave

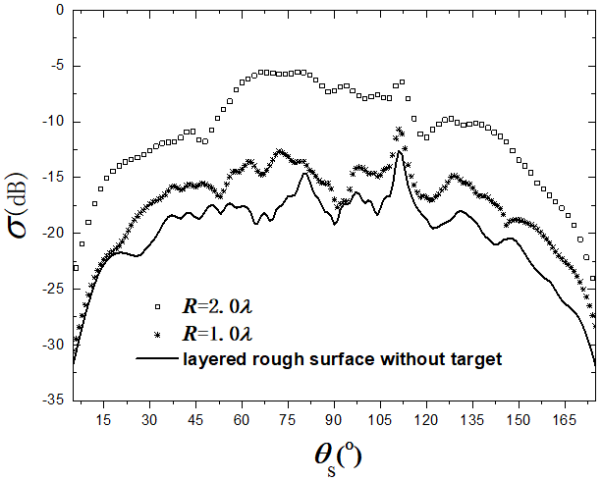

(b) TM incident wave

Fig. 5. Effect of target on compound scattering.

B. Effect of target depth on compound scattering

The target depths are set as $dp = 1.0\lambda$, $dp = 2.0\lambda$, $dp = 3.0\lambda$, respectively, and the effects of different

target depths on the target-environment scattering characteristics are investigated. Figure 6 shows that the composite scattering is almost unaffected by the target depth. While keeping the target volume constant, the target depth increases, its coupling with the upper rough surface decreases, and the coupling with the lower rough surface increases, so no big difference appears in general. In contrast, this variation is more pronounced at TM wave incidence.

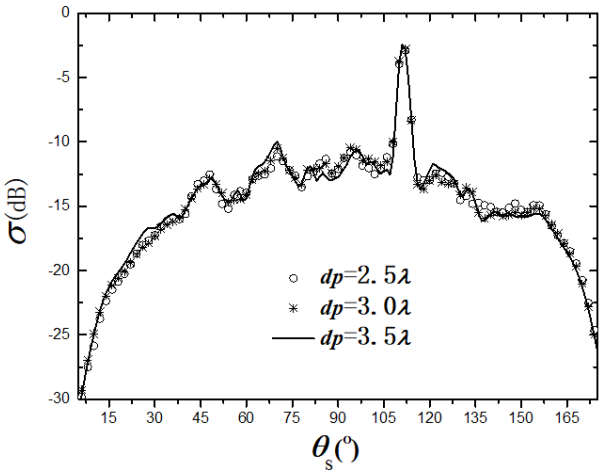

(a) TE incident wave

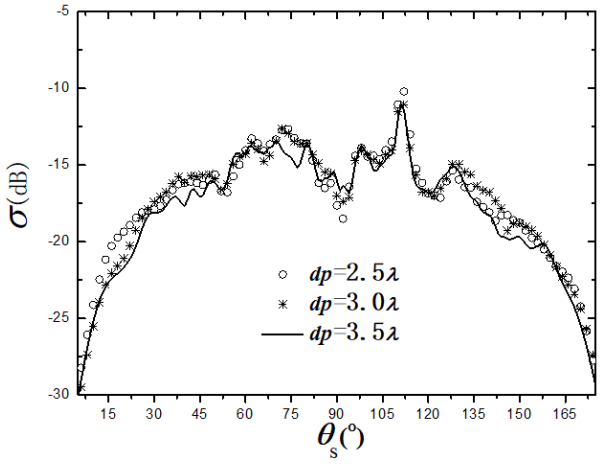

(b) TM incident wave

Fig. 6. Effect of target on compound scattering.

C. The effect of coupling on compound scattering

In this subsection, the coupling effects of the upper and lower rough surfaces and the rough surface-target coupling are mainly discussed. First, the scattering characteristics of a monolayered rough surface with dielectric constant $\varepsilon_{r1} = 4.0 + 0.01i$ are investigated, and the scattering coefficients are calculated for no rough surface-rough surface coupling and no rough surface-target coupling; then, keeping other parameters constant, a second layer of rough surface with dielectric constant $\varepsilon_{r2} = 4.0 + 0.01i$ is set at depth $d = 6.0\lambda$, and the scattering coefficients are calculated for only the rough surface-rough surface coupling action. Keeping the parameters unchanged, a dielectric target is next introduced in the upper rough surface with target depth $dp = 3.0\lambda$, $R = 1.0\lambda$, and dielectric constant $\varepsilon_c = 4$. The scattering coefficient is calculated again when multiple coupling exists. The scattering characteristic curves of the above three cases are shown in Fig. 7.

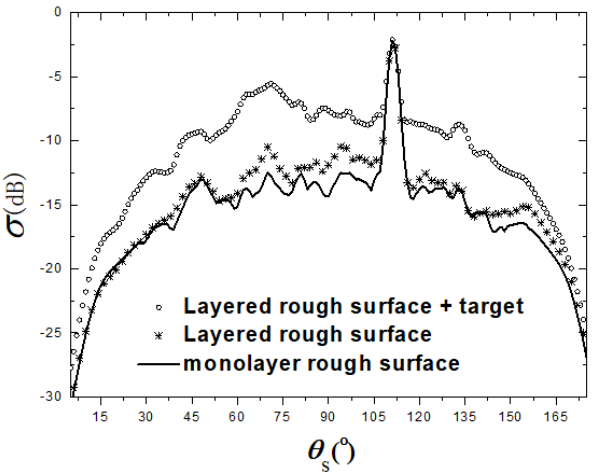

Fig. 7. The effect of coupling on compound scattering.

Figure 7 illustrates that the scattering coefficient of the layered rough surface increases significantly (compared to the single-layer rough surface) due to the coupling between the layers. This indicates that the coupling between the upper and lower layers is also an important component of the layered rough surface. The scattering coefficient continues to increase after the target is buried in the rough surface. It can be seen that the second magnitude is significantly stronger than the first one, indicating a strong coupling effect between the rough surface and the target. When studying electromagnetic scattering in complex environments, ignoring this coupling effect will lead to large errors.

D. ACF (Angular Correlation Function) characteristics for composite environments

The study of ACF is also an important part of the study of scattering in a composite environment. Its expression is [24]

$$\begin{aligned}&\Gamma(\theta_{s1},\theta_{i1},\theta_{s2},\theta_{i2})\\&= \langle \psi_s(\theta_{s1},\theta_{i1})\cdot\psi_s^*(\theta_{s2},\theta_{i2})\rangle / \sqrt{W_1 W_2}\\&= \frac{1}{N_r}\sum_{q=1}^{N_r}\psi_s(\theta_{s1},\theta_{i1},q)\cdot\psi_s^*(\theta_{s2},\theta_{i2},q)/\sqrt{W_1 W_2}. \quad (35)\end{aligned}$$

Where

$$W_1 = \sqrt{\frac{\pi}{2}} g \cos\theta_{i1} \left(1 - \frac{1 + 2\tan^2\theta_{i1}}{2k_0^2 g^2 \cos^2\theta_{i1}}\right), \quad (36)$$

$$W_2 = \sqrt{\frac{\pi}{2}} g \cos\theta_{i2} \left(1 - \frac{1 + 2\tan^2\theta_{i2}}{2k_0^2 g^2 \cos^2\theta_{i2}}\right). \quad (37)$$

Finally, the ACFs of the layered rough surface and the buried target layered rough surface were calculated and plotted in Fig. 8. Figure 8 illustrates that when there is no target, the ACF amplitude of the rough surface is relatively small (less than 0.05). After the target is buried in the rough surface, the scattering at this time consists of both the rough surface and the target, and the ACF amplitude increases significantly and is positively correlated with the size of the target. While changing the burial depth of the target with the same size of the target, the ACF amplitude gradually decreases with the increase of the target depth, which is due to the increase of the target depth and the decrease of his interaction with the rough surface. The graphical results show that the target size is an important factor affecting the ACF, and the ACF can well suppress the scattering from the rough surface and make the scattering characteristics of the target more significant, which is important for the detection of subsurface targets.

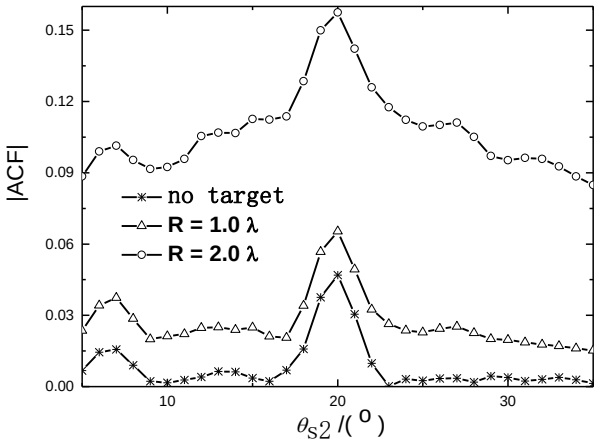

(a) TM incident wave

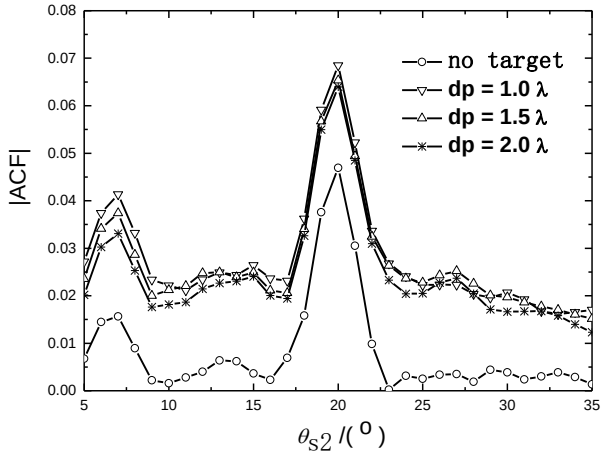

(b) TM incident wave

Fig. 8. ACF characteristics for different conditions.

V. CONCLUSION

This paper focuses on the composite scattering characteristics of layered rough surfaces and buried targets. Firstly, the CCIA algorithm model is established, the EEIF of the rough surface with the target are calculated by FBM and BI-CG respectively, and the coupling effect is realized by continuously updating the excitation term. By comparing the results with those of MOM, it is proved that the computational accuracy and computational speed of CCIA meet the requirements of practical calculations. Then the compound scattering coefficients of the rough surface with the target are calculated by this algorithm, it is found that the coupling effect between them has a great influence on the compound scattering and is positively correlated with the size of the target. It is also found that the burial depth of the target has little effect on the composite scattering characteristics due to the coupling effect between the target with the upper-lower rough surfaces. Finally, its ACF is studied, it is found that the target size is an important factor affecting the ACF, and the ACF can well suppress the scattering from the rough surface and make the scattering characteristics of the target more significant, which is important for detecting subsurface targets.

ADDITIONAL STATEMENTS

There are no conflicts of interest to disclose for all the authors.

REFERENCES

[1] S. Dey, W. G. Szymczak, A. Sarkissian, and J. A. Bucaro, "Scattering from targets in three-dimensional littoral and surf-zone environments with multi-layered elastic sediments based on an interior-transmission formulation," *Computer Methods in Applied Mechanics and Engineering*, vol. 260, 2013.

[2] X. W. Liu, J. Z. Li, Y. Zhu, and S. J. Zhang, "Scattering characteristic extraction and recovery for multiple targets based on time frequency analysis," *Applied Computational Electromagnetics Society (ACES) Journal*, vol. 35, no. 8, 2020.

[3] J. Li, H. G. Bao, and D. Z. Ding, "Analysis for scattering of non-homogeneous medium by time domain volume shooting and bouncing rays," *Applied Computational Electromagnetics Society (ACES) Journal*, vol. 36, no. 3, 2020.

[4] K. Williams, A. Espana, S. Kargl, and M. Zampolli, "Submerged target scattering: comparison of combined finite element/simplified acoustics models to data," *The Journal of the Acoustical Society of America,* vol. 131, no. 4, 2012.

[5] A. Edirisinghe, G. E. Chapman, and J. P. Louis, "A simplified method for retrieval of ground level reflectance of targets from airborne video imagery," *International Journal of Remote Sensing,* vol. 22, no. 6, 2001.

[6] Remote Sensing, "New remote sensing data have been reported by researchers at Fudan university (an analytical method for high-frequency electromagnetic scattering of arbitrary undulating rough surfaces)," *Electronics Newsweekly*, 2020.

[7] P. P. Huang, Q. Shi, W. X. Tan, W. Xu, and C. F. Hu, "Research on modelling and calculation method of river ice electromagnetic scattering," *The Journal of Engineering,* vol. 2019, no. 21, 2019.

[8] Earth Observations and Remote Sensing, "Studies from Xidian university in the area of earth observations and remote sensing reported (spectral decomposition modeling method and its application to EM scattering calculation of large rough surface with SSA method)," *Journal of Technology & Science,* 2015.

[9] E. Bahar and P. E. Crittenden, "Electromagnetic wave scattering from a rough interface above a chiral medium: Generalized telegraphists' equations," *Journal of the Optical Society of America. A, Optics, Image Science, and Vision,* vol. 30, no. 3, 2013.

[10] W. Kong, X. Yang, F. Zhou, J. Xie, C. Chen, N. Li, and W. Yang, "Fast analysis of broadband electromagnetic scattering characteristics of electrically large targets using precorrected fast fourier transform algorithm based on near field matrix interpolation method," *Applied Computational Electromagnetics Society (ACES) Journal*, vol. 36, no. 7, 2021.

[11] D. Sevket, K. Ozkan, and O. Caner, "Interpretation and analysis of target scattering from fully-polarized ISAR images using Pauli decomposition scheme for target recognition," *IEEE Access,* vol. 8, 2020.

[12] P. J. Li and A. W. Wood, "Electromagnetic Scattering by Multiple Cavities Embedded in the Infinite 2D Ground Plane," *Applied Computational Electromagnetics Society (ACES) Journal*, vol. 29, no. 7, 2014.

[13] B. Y. Ding, G. J. Wen, X. H. Huang, C. H. Ma, and X. L. Yang, "Target recognition in synthetic aperture radar images via matching of attributed scattering centers," *IEEE Journal of Selected Topics in Applied Earth Observations and Remote Sensing,* vol. 10, no. 7, 2017.

[14] G. X. Zou, C. M. Tong, H. L. Sun, and P. Peng, "Research on electromagnetic scattering characteristics of combined conducting and dielectric target above coastal environment," *IEEE Access,* vol. 8, 2020.

[15] Y. Liang and L. X. Guo, "A study of composite scattering characteristics of movable/rotatable targets and a rough sea surface using an efficient numerical algorithm," *IEEE Transactions on Antennas and Propagation,* vol. 69, no. 7, 2021.

[16] G. X. Zou, C. M. Tong, J. Zhu, H. L. Sun, and P. Peng, "Study on composite electromagnetic scattering characteristics of low-altitude target above valley composite rough surface using hybrid SBR-EEC method," *IEEE Access,* vol. 8, 2020.

[17] J. X. Li, M. Zhang, W. Q. Jiang, and P. B. Wei, "Improved FBAM and GO/PO method for EM scattering analyses of ship targets in a marine environment," *Sensors,* vol. 20, no. 17, 2020.

[18] M. Wang, J. Chen, and Y. Cao, "An efficient scheme for analysis of electromagnetic scattering from target and environment composite model," *Progress in Electromagnetics Research M.,* vol. 32, 2013.

[19] C. D. Moss, T. M. Grzegorczyk, H. C. Han H, and J. A. Kong, "Forward-backward method with spectral acceleration for scattering from layered rough surfaces," *IEEE Trans Antennas Propagation,* vol. 54, no. 3, 2006.

[20] K. C. Wang, Z. He, D. Z. Ding, and R. S. Chen, "Uncertainty scattering analysis of 3-D objects with varying shape based on method of moments," *IEEE Transactions on Antennas and Propagation,* vol. 67, no. 4, 2019.

[21] M. A. Mojtaba, S. S. H. Hesamedin, and D. Mojtaba, "A method of moments for analysis of electromagnetic scattering from inhomogeneous anisotropic bodies of revolution," *IEEE Transactions on Antennas and Propagation,* vol. 66, no. 6, 2018.

[22] J. Y. Li and L. W. Li, "Electromagnetic scattering by a mixture of conducting and dielectric objects: Analysis using method of moments," *IEEE Transactions on Vehicular Technology,* vol. 53, no. 2, 2004.

[23] A. Thorsos, "The validity of the Kirchhoff approximation for toygh surface scattering using a Guassian roughness spectrum," *Journal of the Acoustical Society of America,* vol. 83, no. 1, 1988.

Jiaguo Zhang was born in Jiangxi, China. He received a bachelor's degree from Yichun University in 2011 and a master's degree of computer technology from Yunnan University in 2016. Her research interests include network technology and computer communication.

Huan Wei was born in Jiangxi, China. He received a bachelor's degree from Zhejiang University in 2005 and a master's degree of computer technology from Yunnan University in 2015. Her research interests include network technology and computer communication.